Interaction between self-interstitials and substitutional C in silicon: Interstitial trapping and C clustering mechanism

S. Mirabella
INFM and Dipartimento di Fisica e Astronomia, Università di Catania, Corso Italia 57, 95129 Catania, Italy

A. Coati, D. De Salvador, E. Napolitani, A. Mattoni, G. Bisognin, M. Berti, A. Carnera, and A. V. Drigo
INFM and Dipartimento di Fisica, Università di Padova, Via Marzolo 8, 35131 Padova, Italy

S. Scalese, S. Pulvirenti, A. Terrasi, and F. Priolo
INFM and Dipartimento di Fisica e Astronomia, Università di Catania, Corso Italia 57, 95129 Catania, Italy
(Received 15 August 2001; published 11 January 2002)

In this work the Si self-interstitial–carbon interaction has been experimentally investigated and modeled. The interactions between self-interstitials, produced by 20-keV silicon implantation, and substitutional carbon in silicon have been studied using a $Si_{1-y}C_y$ layer grown by molecular beam epitaxy (MBE) and interposed between the near-surface self-interstitial source and a deeper B spike used as a marker for the Si-interstitial concentration. The C atoms, all incorporated in substitutional sites and with a C-dose range of $7\times10^{12}-4\times10^{14}$ atoms/cm^2, trap the self-interstitials in such a manner that the $Si_{1-y}C_y$ layer behaves as a filtering membrane for the interstitials flowing towards the bulk and, consequently, strongly reduces the boron-enhanced diffusion. This trapping ability is related to the total C dose in the $Si_{1-y}C_y$ membrane. Substitutional carbon atoms interacting with self-interstitials are shown to trap Si interstitials, to be removed from their substitutional sites, and to precipitate into the C-rich region. After precipitation, C atoms are not able to further trap injected self-interstitials, and the interstitials generated in the surface region can freely pass through the C-rich region and produce B-enhanced diffusion. The atomistic mechanism leading to Si-interstitial trapping has been investigated by developing a simulation code describing the migration of injected interstitials. The simulation takes into account the surface recombination, the interstitial diffusion in our MBE-grown material, and C traps. Since the model calculates the amount of interstitials that actually react with C atoms, by a comparison with the experimental data it is possible to derive quantitative indications of the trapping mechanism. It is shown that one Si interstitial is able to deactivate about two C traps by means of interstitial trapping and C clustering reactions. The reaction causing trapping and deactivation is tentatively described.

DOI: 10.1103/PhysRevB.65.045209 PACS number(s): 61.72.Tt, 66.30.Jt, 81.15.Hi

I. INTRODUCTION

The study of point defects in crystalline silicon and their interactions with the most commonly used dopants has been in the past decades, and still nowadays represents, one of the most crucial topics in the semiconductor scientific community.[1–8] For example, it has been demonstrated that, under equilibrium conditions, B diffuses exclusively via a process involving the interaction with a silicon self-interstitial (I) though the precise atomistic mechanism is still under strong debate.[9–11]

A consequence of such mechanisms is that changes in the equilibrium populations of the intrinsic defects cause deviations from the equilibrium diffusion coefficients of the dopants. Nonequilibrium diffusion has gained large interest because of its implications on advanced microelectronic technology.[12–15] In fact, some of the most important microelectronic production steps, such as ion implantation and thermal oxidation, cause interstitial supersaturation (i.e., interstitial concentration higher than the equilibrium one), which gives rise to anomalous diffusion of the dopants reported to as transient-enhanced diffusion (TED) and oxidation-enhanced diffusion (OED) in the case of ion implantation and thermal oxidation, respectively. These physical mechanisms are some of the limiting steps towards the scaling down of device size. For example, during the postimplantation annealing necessary for the electrical activation, a large broadening of the implanted boron profile occurs that is detrimental for the dopant confinement and ultrashallow junction formation. On the other hand, the interstitial-induced diffusion of B can be used as a sensitive tool to investigate the I flux evolution in the different experimental conditions.[2,16]

As for boron, even carbon has an interstitial diffusivity fraction close to one.[17] The basic mechanism of carbon diffusion is the so-called ''kick-out'':[12,18]

$$I + C_s \rightarrow C_i ,$$

in which a self-interstitial (I) pushes out a carbon atom from a substitutional site (C_s), creating a highly mobile interstitial carbon (C_i); even the dissociative Frank-Turnbull mechanism is shown to be possible,[19] in which a substitutional carbon turns itself into an interstitial form, leaving a vacancy in its original site. For the first time, 25 years ago, Watkins and Brower[20] showed by electron paramagnetic spectroscopy that the interstitial carbon (C_i) structure consists of one silicon and one carbon atom pair, partially sharing a single substitutional site.

Independently of the atomistic mechanism responsible for its diffusivity, C appears to be a trap for Si self-interstitials and thus to be able to reduce B diffusivity. This phenomenon was studied both under equilibrium conditions[21,22] and in implanted or oxidized samples,[12,16,23–26] thus introducing *I* supersaturation.

In equilibrium conditions it was shown that a high concentration of C can induce an undersaturation of self-interstitials, strongly reducing thermal diffusion of boron spikes located in C-rich silicon.[22] This was explained in terms of a coupled diffusion of C and Si interstitials that induces undersaturation of interstitials and out-diffusion of C from the C-rich region.[21]

C is effective as an *I* trap also in nonequilibrium conditions. If B is implanted in C-rich silicon, the supersaturation of self-interstitials produced by the ion-implantation process is reduced by C, resulting in a strong B TED suppression.[16,23] Moreover, it has been demonstrated that this suppression increases with increasing overlapping of implanted B and C profiles, and that it is due to the formation of *I* clusters either with B or C atoms. Rücker *et al.*[24] showed the TED suppression of boron spikes grown in C-rich silicon and subjected to BF_2 implantation. Also this effect was explained by C-*I* interaction and C out-diffusion, even if a fraction of immobile C was revealed.

On the other hand, it is known that C in $Si_{1-y}C_y$ and $Si_{1-x-y}Ge_xC_y$ alloys precipitates in clusters visible to transmission electron microscopy (TEM) under thermal annealing.[27,28] Moreover, competition between C diffusion and C clustering under interstitial injection by thermal oxidation has been demonstrated.[29] Finally, the existence of C_iC_s carbon pairing was characterized in low C concentrations in Si.[30] However, the use of such a mechanism (C_iC_s) for explaining the *I* trapping phenomenon was recently proposed also for high C concentrations in Si.[31] The results above suggest that the *I*-trapping mechanism involves very complex phenomena and that the C out-diffusion could not be the only mechanism involved but also C clustering and/or C precipitation should be taken into account.

The C-B interaction and the electrical deactivation of B in the C-rich region[12,32] can be avoided by spatially separating the C layer from B. In fact, suppression of B TED and OED by $Si_{1-x-y}Ge_xC_y$ layers was observed recently even with a carbon-rich silicon layer well separated from the B spike used to monitor the *I* supersaturation.[25] Moreover, the ability of a remote $Si_{1-y}C_y$ layer to suppress the TED of B implanted in preamorphized silicon was demonstrated.[26]

In this paper we study the effect of a $Si_{1-y}C_y$ layer placed between a deep B spike and a surface implanted region (Si cap layer) on the TED of the deep B spike. Moreover, we characterized the evolution of both the carbon-concentration profile and its lattice location under the interstitial wind. In our conditions of high *I* flux, C clustering will be shown to be predominant with respect to C out-diffusion. Moreover, clustered C will be shown to be no longer active as an interstitial trap. From our experimental results it turns out that some of the possible interaction mechanisms can be neglected and a simplified model able to quantify the number of interstitials reacting with the $Si_{1-y}C_y$ layer will be proposed. Such a model takes into account the *I* loss through the surface, the intrinsic *I* traps present in molecular beam epitaxy (MBE)–grown Si (Refs. 4 and 16), and the *I*-C interactions. The use of the model to reproduce the experimental data leads to the conclusion that one self-interstitial produces the deactivation of two C atoms. An atomistic interpretation of the result above is also proposed.

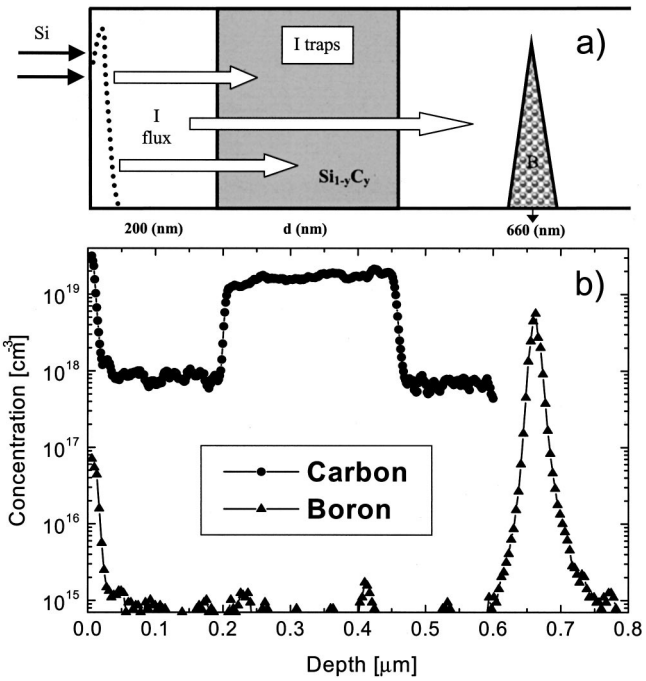

FIG. 1. (a) Schematic description of the experiment: the Si structure used contains a B spike at a depth of 660 nm and a $Si_{1-y}C_y$ layer, of variable thickness *d*, below a 200-nm-thick Si cap layer; (b) SIMS profiles of B and C concentration incorporated in one of our samples ($d=250$ nm, $y=0.03$ at. %).

II. EXPERIMENT

In order to study the interactions between Si self-interstitials produced by Si implantation and substitutional carbon in silicon, a sample structure whose schematic is drawn in Fig. 1(a) was prepared by MBE. We grew a 850-nm-thick Si structure on a 2×1 reconstructed Si(100) surface. The substrate temperature was kept at 500 °C during the growth while the Si rate deposition was 1 Å/s. The base pressure measured in the MBE chamber was $\sim5\times10^{-11}$ mbar. The Si structure contains a B spike, inserted at a depth of 660 nm with a peak concentration of $\sim6\times10^{18}$ B/cm^3 and a full width at half maximum of about 8 nm, while a $Si_{1-y}C_y$ layer was placed 200 nm below the sample surface (Si cap layer). A similar structure without carbon was also grown, as a reference sample. The role of the B spike is that of acting as a marker for the interstitial flux. The C fraction was varied in the range 0.01–0.03 at. %, while the $Si_{1-y}C_y$ layer thickness (*d*) was varied between 10 and 250 nm, resulting in a total C dose incorporated in our samples ranging from 7×10^{12} to 4×10^{14} C/cm^2.

The chemical concentration depth profiles of C and B

were obtained by secondary-ion mass spectrometry (SIMS), using a CAMECA IMS-4*f* instrument. A 300-nA, O_2^+ analyzing beam was used, rastered over an area of 250 $\times 250\,\mu m^2$, while collecting C^+ and B^+ ions from a central area of 60 μm in diameter. The samples were biased at +4.5 kV, and the primary-beam impact energy was 3 keV. In these conditions, the detection limit of B and C was below 1×10^{15} and 1×10^{18} atoms/cm^3, respectively. The background C contamination in the MBE silicon layers was measured using 14.5-keV Cs^+ primary-ion and C^- secondary-ion detection, thus lowering by one order of magnitude the C detection limit, at the cost of a poorer depth resolution.

To have a quantitative measure of the total substitutional carbon dose, strain analyses by high-resolution x-ray diffraction (HRXRD) were performed.[33,34] HRXRD measurements were collected with a Philips diffractometer with a Bartels Ge(220) four-crystal monochromator, using a channel-cut Ge(220) analyzer before the detector (triple-axis configuration). The sample illuminated area was of about $1\times10\,mm^2$. The strain profile was obtained by means of dynamical x-ray scattering theory simulations based on the Takagi-Taupin equations.[35] To this aim (004) rocking curves were analyzed following the strain-substitutional C relationship described in Refs. 33 and 34. The minimum substitutional carbon dose detectable in the present structures turns out to be about $(0.5-1)\times10^{13}$ C/cm^2. High-resolution x-ray diffraction analyses revealed that the C atoms were fully substitutional in the as-grown samples.

In Fig. 1(b) we show the grown structure plotting the O_2^+ primary-ions SIMS concentration profiles of C (●) and B (▲) incorporated in one of our samples ($d=250$ nm, $y=0.03$ at. %). The carbon contamination out of the $Si_{1-y}C_y$ region grown on purpose was measured, by means of the Cs^+ primary-ion beam, to be much lower (2×10^{17} C/cm^3) than the detection limit obtained in the measurement conditions of Fig. 1(b). Ion implantation of 20-keV Si was then performed on these samples at doses of 2×10^{13}, 5×10^{13}, and 1×10^{14} ions/cm^2 in order to introduce a controlled amount of Si interstitials. The implant damage region was always contained in the Si cap layer, and moreover all of the implant doses were well below the amorphizing threshold. Finally, all the samples, as-grown and implanted ones, were subjected to rapid thermal annealing (RTA) at a temperature of 800 °C for a time long enough to extinguish the transient-enhanced diffusion of boron for each implant dose: this condition is fully satisfied for a time of 5, 5, and 10 min for the three implant doses, respectively. Furthermore, TEM analyses (not reported here) confirmed that all the extended defects formed during the ion implantation were dissolved after the RTA process. Therefore, the whole implantation damage is the source of interstitials migrating from the damaged region towards the surface and the bulk.

III. RESULTS

A. Reduction of B transient-enhanced diffusion

The postimplant annealing, as it is known,[12] induces the agglomeration and successive evaporation of {311} defect clusters in such a manner that interstitials diffuse from the ion-implanted damaged region towards the surface and the bulk of the material. An interstitial concentration orders of magnitude higher than the equilibrium value can be reached for a transient time, in which chemical species that have a high interstitial fraction of diffusivity,[8] such as boron, undergo an enhanced diffusion process (TED). In our case, the phenomenon above can be seen in Fig. 2, where the boron concentration profile obtained by SIMS analyses is plotted for samples implanted with 20-keV Si at the highest dose, 1×10^{14} ions/cm^2, and annealed at 800 °C for 10 min. The continuous line (—) is the profile of the B spike in the as-grown reference sample, which does not contain C but is equivalent to the other samples both in the width and depth of the B spike. The open circles (○) represent the spike annealed at 800 °C for 5 min without any implant: The thermal broadening of the profile is very small; in fact the mean diffusion length, $L=(D_B^{eq}t)^{1/2}$, using the boron equilibrium diffusivity D_B^{eq} taken from Fair,[36] is <2 nm. The TED of the boron spike, for the implanted samples, is visible in the profiles plotted with filled symbols: the largest broadening is obtained in the reference sample (no C, ●), as expected if we assume that C acts as a trap for Si interstitials.

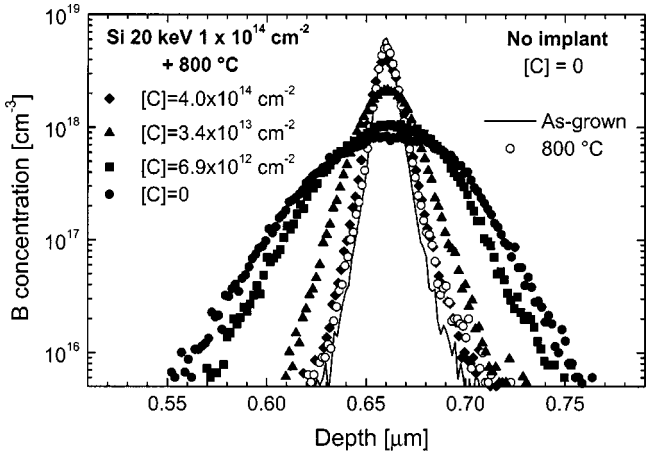

FIG. 2. SIMS profiles of the B spike. The line (—) and the open circles (○) are the reference samples as-grown and annealed at 800 °C, respectively. The solid symbols refer to 20-keV 1×10^{14} cm^{-2} Si implanted and 800 °C annealed samples with different C doses: 4×10^{14} C/cm^2 (♦), 3.4×10^{13} C/cm^2 (▲), 6.9×10^{12} C/cm^2 (■) and reference, no C (●).

The effect of the $Si_{1-y}C_y$ membrane on the boron-enhanced diffusion depends on the total carbon dose: For the lowest carbon dose, 6.9×10^{12} atoms/cm^2 (■), we obtain a slight reduction of B TED with respect to the reference sample (no C), while for the highest dose, 4.0×10^{14} atoms/cm^2 (♦), an almost complete suppression of the enhanced diffusion is registered. So, during the postimplant annealing the migration of interstitials from the ion-implanted damaged region towards the deep B spike is affected by the presence of a $Si_{1-y}C_y$ layer that clearly acts as a membrane, filtering the interstitial flow. The ability of this membrane to trap interstitials increases with the total carbon dose.

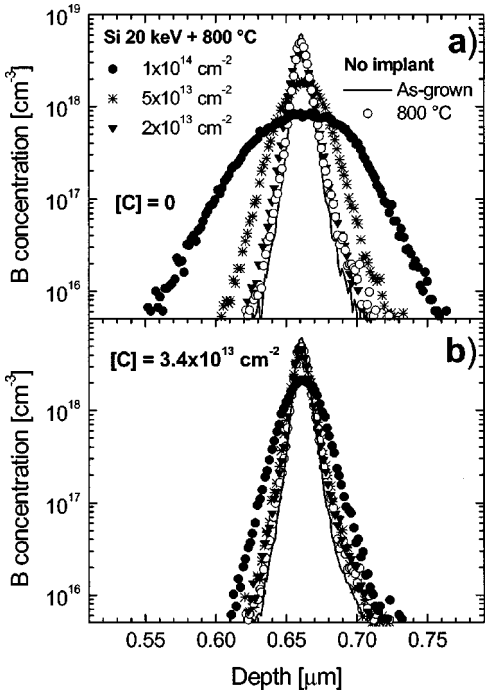

FIG. 3. SIMS profiles of the B spike. (a) and (b) refer to the reference and 3.4×10^{13} C/cm^2 samples: the line (—) and the open circles (○) refer to the as-grown and 800 °C annealed samples, while the effects of 20-keV Si implantation and subsequent annealing are plotted for different implant doses: 1×10^{14} cm^{-2} (●), 5×10^{13} cm^{-2} (*), 2×10^{13} cm^{-2} (▼).

The effect of the implantation fluence on the boron TED was then studied both in the reference structure and in the medium carbon dose (3.4×10^{13} C/cm^2) sample and the results are shown in Figs. 3(a) and 3(b), respectively. In Fig. 3(a) the results relative to the reference sample (no C) are reported: as expected, the larger the implantation fluence, the larger the broadening of the boron spike. However, for the lowest implantation fluence (2×10^{13} ions/cm^2,▼), nearly no broadening is observed with respect to the simple thermal treatment (○). We can deduce that the migration of interstitials towards the bulk is not able to reach the depth of the B spike (660 nm) and to produce there a self-interstitial concentration higher than the equilibrium value. In some way there is a threshold in the implant dose: this effect can only be due to the presence of *I* traps in the as-grown MBE silicon material. By looking at Fig. 3(b) it appears that the effect of C is to raise this dose threshold above 5×10^{13} ions/cm^2. As a matter of fact, after implantation of this dose the boron broadening (*) is comparable to the pure thermal effect (○), while the 1×10^{14} ions/cm^2 implantation fluence (●) is only slightly larger than the thermal one and much smaller than that in the reference sample. It appears that our $Si_{1-y}C_y$ layer with 3.4×10^{13} C/cm^2 behaves as an opaque membrane for low implantation doses, preventing *I* from reaching the boron spike. For the highest implant dose the $Si_{1-y}C_y$ membrane becomes semitransparent to the interstitial flow and nonequilibrium boron diffusion is registered.

The boron peak broadening is used in order to measure the interstitial supersaturation during the TED process. The

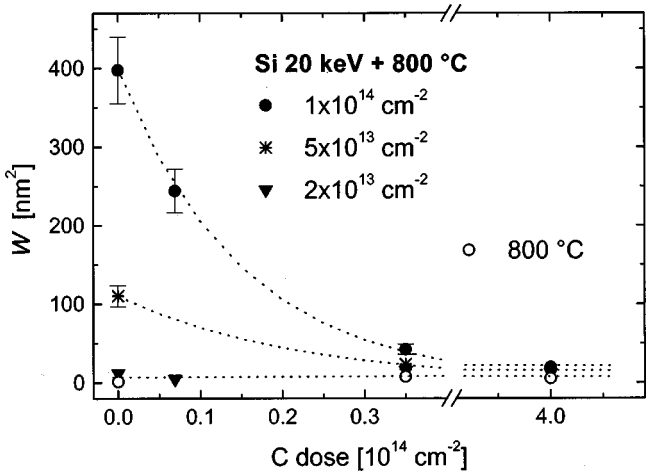

FIG. 4. Broadening of the B spike vs total C dose for different implant doses: 1×10^{14} cm^{-2} (●), 5×10^{13} cm^{-2} (*), 2×10^{13} cm^{-2} (▼). The open circles (○) represent pure thermal broadening. The dotted lines (···) are guides for eyes.

information about the supersaturation is extracted as follows. The variances of the as-grown (σ_0^2) and post-TED (σ^2) B peaks are directly calculated by the SIMS concentration distributions after background subtraction. The difference of such variances $\sigma^2-\sigma_0^2$ is the variance of the boron distribution after deconvolution with the as-grown profile. Cowern and co-workers[2] demonstrated that, even if in general the B broadening does not have a Gaussian shape due to the kick-out mechanism, the variance of the B distribution is related to the *I* supersaturation being equal to the quantity $2D_B^{eq}\int(c_I/c_I^{eq})dt$ (where c_I and c_I^{eq} are the interstitial concentration at time *t* and the equilibrium one, respectively). In the following we will use the integrated diffusivity *W*, defined as follows, to identify the effective B diffusivity integrated over the TED time:

$$W=\frac{\sigma^2-\sigma_0^2}{2}=D_B^{eq}\int\frac{c_I}{c_I^{eq}}dt. \tag{1}$$

The results of such an exercise are shown in Fig. 4, where the integrated diffusivity is plotted as a function of the total carbon dose for the different implant doses, together with the case of no implant (○); the dotted lines (···) are only guides for the eyes, while the error bars, when not drawn, are to be considered lower than the size of the symbols. As just observed, the effect of the lowest implant dose (2×10^{13} ions/cm^2,▼) on the B-spike broadening is indistinguishable from that measured after the pure thermal annealing (○), and this is true for all carbon doses. We can state that the horizontal dotted line represents the mean value for the experimental integrated diffusivity under equilibrium conditions. If the implant dose is increased to 5×10^{13} ions/cm^2 (*) or to 1×10^{14} ions/cm^2 (●), we measure an increasing broadening with respect to the equilibrium condition. This effect becomes smaller the higher the total carbon dose, and it vanishes for the highest C dose (4×10^{14} cm^{-2}): for this case none of the investigated implant doses produces spike broadening distinguishable from the

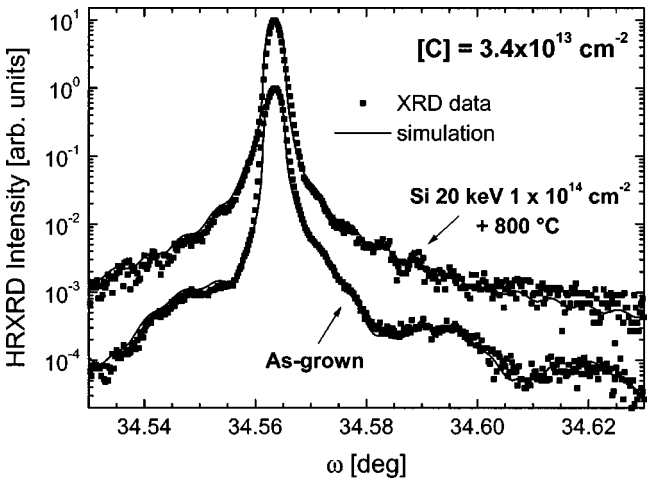

FIG. 5. HRXRD spectra (■) for the 3.4×10^{13} C/cm^2 as-grown sample (lower spectrum) and 20-keV 1×10^{14} cm^{-2} Si implanted and annealed sample (upper spectrum). The data are well fitted by simulations (—) assuming all the C atoms are in substitutional sites for the as-grown sample and out of these sites in the other case.

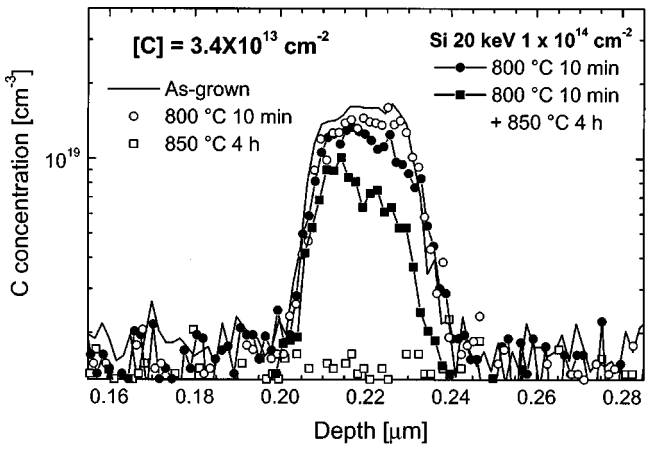

FIG. 6. SIMS profiles of C in the 3.4×10^{13} C/cm^2 sample: the line (—) refers to the as-grown sample, while the closed symbols are the C profile after 20-keV 1×10^{14} cm^{-2} Si implantation and annealing at 800 °C for 10 min (●) and at 850 °C for 4 h (■). The relative open symbols refer to pure thermally annealed samples.

equilibrium one; this means that the $Si_{1-y}C_y$ membrane, because of its large carbon dose, remains totally opaque to the interstitial flow.

The $Si_{1-y}C_y$ layer interposed between the interstitial source and the deep B spike behaves as a filter for the interstitial flow with the consequence of reducing the TED of boron. This TED reduction depends on the total C dose in the $Si_{1-y}C_y$ membrane and could become a full suppression of the enhanced diffusion in the case of a high enough C dose. Furthermore, we observed a threshold for the implantation dose in order to observe an enhanced diffusion in the B spike at the depth of 660 nm, and we attribute this phenomenon to the presence of intrinsic traps for interstitials in the MBE-grown material.

B. Self-interstitial–carbon interaction

In order to understand the behavior of C atoms under the interstitial flow generated by the Si implantation, we studied in detail the sample with the medium carbon dose (3.4×10^{13} C/cm^2). In Fig. 5 the high-resolution x-ray diffraction data relative to the as-grown (lower spectrum) and to the 1×10^{14} Si/cm^2 implanted and annealed sample (upper spectrum) are plotted (■) together with their best simulations (—). For HRXRD dynamical theory simulations the relevant parameters used are the substitutional C concentration and the thicknesses of the $Si_{1-y}C_y$ film and of the Si cap layer. For the as-grown sample (lower spectrum) the HRXRD data are satisfactorily simulated by assuming all the incorporated carbon (SIMS profile) to be substitutional. The same result was obtained for all the samples grown with different C doses. Moreover, HRXRD analyses (not shown) revealed that, in all of the samples, no loss of substitutional carbon occurred after the pure thermal annealing at 800 °C. So, all the carbon atoms incorporated during the MBE growth are substitutional, even after a pure thermal treatment in equilibrium conditions.

A satisfactory simulation of the same sample implanted with 1×10^{14} Si/cm^2 after annealing (Fig. 5, upper spectrum) is obtained by assuming no strain due to C, which means that either C is completely out-diffused or C is no longer on substitutional sites as we expect if the trapping reaction $I+C_s\rightarrow C_i$ occurs.[12,37] In fact, for this implant dose we saw [Fig. 3(b)] that the migration of interstitials towards the bulk reaches the B spike by passing through the $Si_{1-y}C_y$ membrane. The HRXRD analysis clearly indicates that the interstitial flow, as a result of the trapping reaction, has strongly modified the original arrangement of the carbon atoms. Furthermore, HRXRD analysis (not shown) performed on the same sample revealed an almost full loss of substitutional carbon (strain) after the implantation of 5×10^{13} Si/cm^2 and annealing, while for the lowest implant dose (2×10^{13} Si/cm^2) the loss of carbon substitutionality is limited to one-third of the total carbon dose. On the basis of the results discussed so far, we can state that whenever the injected self-interstitials arrive at the substitutional carbon, carbon loses its original substitutional position and no longer contributes to the measured strain.

In order to investigate the behavior of the carbon atoms that have interacted with the self-interstitials and lost their substitutional sites, we performed SIMS analyses on the medium carbon dose sample after implantation and/or annealing. The results are reported in Fig. 6, where the as-grown C profile is the continuous line (—), while the circles refer to a rapid thermal annealing at 800 °C for 10 min performed on the as-grown sample (○) or on the 1×10^{14} Si/cm^2 implanted sample (●). As it clearly appears, both the thermal process and the implantation and annealing process do not induce appreciable carbon diffusion: both C profiles after the annealing processes, the open (○) and the closed circles (●), nearly overlap the as-grown sample. On the other hand, for these samples we just saw, by HRXRD analysis (Fig. 5), that the thermal process does not move the carbon from its substitutional position. However, the implantation and annealing process leads to a total loss of C-induced strain. Therefore,

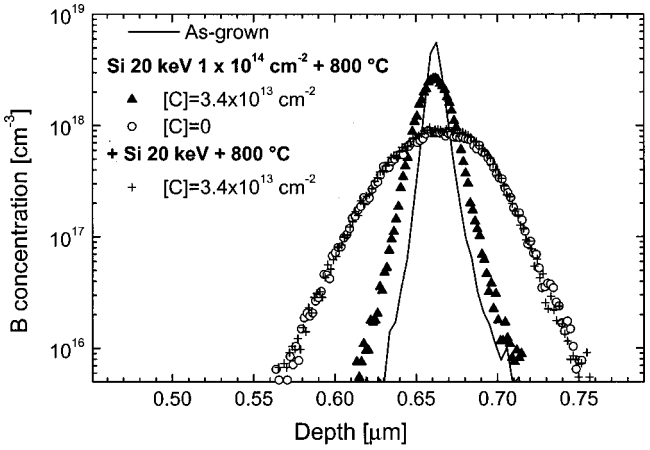

FIG. 7. SIMS profiles of the B spike. The line (—) is the as-grown sample. The effect on the B spike of a 20-keV $1\times10^{14}\,\mathrm{cm}^{-2}$ Si implantation and subsequent annealing at 800 °C for 10 min is plotted for the reference sample (○) and for the 3.4 $\times10^{13}\,\mathrm{C/cm}^2$ sample (▲). A double implantation plus annealing process in the C-rich sample leads to the B profile plotted by crosses (+).

the self-interstitials interact with the substitutional carbon atoms in such a manner that they remove C from the substitutional sites, but, once removed, the C atoms are not able to significantly diffuse out of the $Si_{1-y}C_y$ layer.

In order to test the thermal stability of the carbon atoms blocked into the $Si_{1-y}C_y$ layer in the sample implanted with $1\times10^{14}\,\mathrm{Si/cm}^2$ and annealed, we further processed the sample in a furnace at 850 °C for 4 h in N_2 atmosphere. The SIMS profile is shown in Fig. 6 by closed squares (■). Most of the C atoms remain in the $Si_{1-y}C_y$ layer, indicating a great stability of this precipitated/clustered carbon, in contrast with the diffusion that would cause the disappearance of the original C box in the case of equilibrium condition. In fact, in Fig. 6 the open squares (□) refer to the C profile of an as-grown sample annealed at 850 °C for 4 h without any implantation. In this case C has fully disappeared by diffusing into the sample. Moreover, HRXRD measurements show that the precipitated C remains nonsubstitutional even after this thermal treatment: This suggests a sort of irreversibility in the C_s precipitation (the C does not return as substitutional once it has interacted with an interstitial).

Up to now we showed the ability of a $Si_{1-y}C_y$ layer to act as a membrane filtering the interstitial migration through the bulk and the loss of substitutional carbon caused by the interaction between the self-interstitials and the substitutional carbon. After this trapping reaction the carbon remains in the original layer region (Fig. 6). In order to investigate the residual trapping capability, if any, of those carbon atoms that have already interacted with self-interstitials and are no longer substitutional, we performed a further Si implantation followed by further annealing at 800 °C on the medium-carbon-dose ($3.4\times10^{13}\,\mathrm{C/cm}^2$) sample previously implanted and annealed. Figure 7 shows the SIMS profiles of the B spike in an as-grown sample (—), after the first implantation and annealing on the reference sample (○) and on the medium-carbon-dose sample (▲), and after the double implantation and annealing process on the carbon sample (+). As we just observed, during the first process the $Si_{1-y}C_y$ layer behaves as a good trap for self-interstitials, while it seems to be almost ineffective for the trapping of the second interstitial flow, producing a B TED (+) similar to that observed in the reference sample after a single implantation and annealing process (○).

Summarizing, substitutional carbon atoms interacting with Si self-interstitials are able to trap them, are removed from their substitutional sites, are forbidden to diffuse and, in this condition, if subjected to a further Si implantation, they are unable to trap implanted self-interstitials.

IV. MODELING AND DISCUSSION

A. Injected interstitial diffusion in MBE silicon

In order to gain further insights into the interaction between C and Si self-interstitials, responsible for the trapping effect described above, we need to quantify the flux of interstitials reaching the C-rich layer. To this aim, the *I* injection by implant and annealing and the *I* diffusion in our material must be first described. In the this section, a model describing the interstitial migration in a test sample without C will be presented; then, in the following section, the model will be properly extended to the case of a sample containing a $Si_{1-y}C_y$ layer.

It is well established that the *I* diffusion in MBE material is mediated by the interaction with intrinsic traps that are present in the material and reduce the effective diffusivity of the interstitials.[2] This phenomenology is satisfactorily described in the case of a constant injection of interstitials through surface oxidation by the rate equations described in Ref. 4.

In order to test and quantify the presence of traps in our material, a test structure with five equally spaced (200-nm) B spikes was grown, implanted, and annealed under the same conditions as for the other samples previously considered. Such an exercise is a useful and commonly used procedure to evaluate the intrinsic trap concentration in the material.[4,12] In Fig. 8(a) the SIMS profiles of the B spikes are reported for the as-grown sample (—) and for the implanted and annealed sample (●). In the first B spike, at 200 nm, the characteristic peak shape reveals the presence of immobile B atoms: This results form the B-*I* clustering due to the proximity of the implanted region.[12] This immobile B fraction does not contribute to the spike broadening and was subtracted from the profile before calculating *W*, similarly to that reported in Ref. 12. The broadening *W* of the B spikes as a function of the depth is reported in Fig. 8(b) as open circles (○). As can be seen, the broadening significantly decreases by increasing the depth, indicating that the *I* diffusion is strongly limited by traps.

The data can be numerically reproduced by solving the following equations, involving the time and spatial evolution for the interstitials and the intrinsic traps concentrations, c_I and c_t respectively:

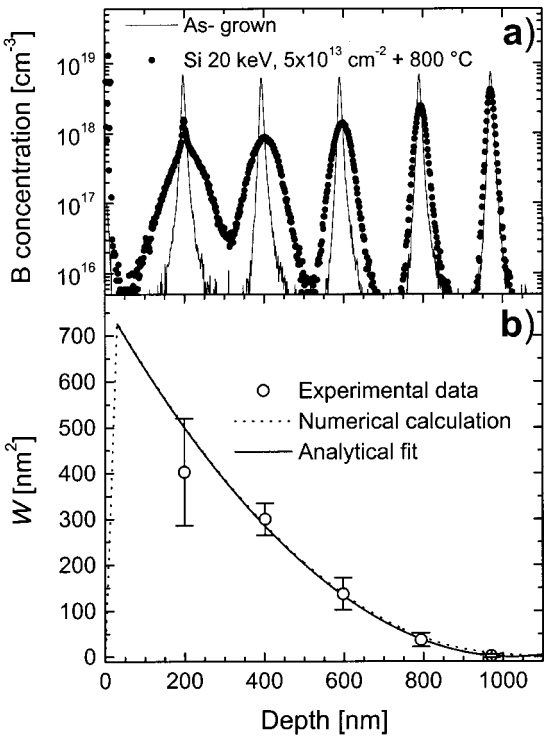

FIG. 8. B spikes. (a) SIMS profile of the B spikes as-grown (—) and after 20-keV $5\times10^{13}\,\mathrm{cm}^{-2}$ Si implantation and subsequent annealing at 800 °C for 5 min (●). (b) Broadening of the B spikes after implantation and annealing (○). The continuous line (—) refers to an analytical fit of the data, while the dotted line (···) is a numerical calculation (see text).

$$\frac{\partial c_I(x,t)}{\partial t}=\nabla(D_I\nabla c_I)-(4\pi a_t D_I c_I c_t-G)+\phi\,\delta(x-r_p)$$

$$-\frac{D_I}{\lambda}(c_I-c_I^{\mathrm{eq}})\,\delta(x), \tag{2a}$$

$$\frac{\partial c_t(x,t)}{\partial t}=-(4\pi a_t D_I c_I c_t-G)/n_t. \tag{2b}$$

Equations (2) are the equations proposed in Ref. 4 by Cowern in order to describe the *I* diffusion when traps are present in the material, with the exception of the third and fourth terms in the right-hand side of Eq. (2a), which are introduced to describe the interstitial injection and surface recombination, respectively.

These equations contain many parameters that must be set in order to obtain a satisfactory fit of the data. The parameters are the capture radius a_t of the *I*-trap interaction, the density of traps at zero time $c_t(x,0)=N_t$, the number of Si interstitials captured by each trap, n_t, and the probability G of *I*-trap backward reaction.[38] Physical constants have to be used, such as the *I* diffusivity D_I and the *I* equilibrium concentration c_I^{eq}. Finally, it is worth noting that in order to relate the model results $[c_I(x,t)]$ to the experimental data (the boron spike broadening *W*) Eq. (1) must be used, passing through the boron equilibrium diffusivity $D_{\mathrm{B}}^{\mathrm{eq}}$.

In addition, the source of Si self-interstitials should be modeled; in fact, in our case, an interstitial injection by ion implantation was used instead of thermal oxidation as in Ref. 4. We assume that the Si implant plus annealing introduces an interstitial flux ϕ, for a given time *T*, at the Si projected range depth r_p [third term in the right-hand side of Eq. (2a), and δ symbol represents the Dirac function]. Moreover, the Si-interstitial interaction with the surface is regulated by an evaporation rate factor D_I/λ as proposed in Ref. 39, where λ is defined as a surface recombination length [fourth term of Eq. (2a)].

The basic idea of Eqs. (2) is that the Si-interstitial atoms both diffuse and react with traps inside the Si matrix. The interaction term $(4\pi a_t D_I c_I c_t)$ causes a reduction of both the interstitial and trap population. As a result, the interstitials are forced to consume the traps before penetrating inside the sample.

We found that Eqs. (2) admit an analytical approximated solution that is very useful in order to understand the dependence of the numerical results on the large number of parameters described above. The basic approximations underlying the analytical solution are the following: (i) the time evolution of the active trap density is described by an edge function $N_t\theta(x-R(t))$, θ being the Heaviside function. N_t is the trap density before the *I*-injection process, *x* is the depth below the surface, and $R(t)$ is the depth at which the active trap density edge is located at the time *t*. This abrupt trap distribution corresponds to the assumption that the mean free path of the interstitials inside the trap zone is negligible. However, we will show that this assumption does not affect the calculation of the B broadening *W*. (ii) The *I* concentration profile evolves through quasistationary states. At each given time, the *I* concentration profile has a triangular shape peaked at the *I*-injection depth r_p and with the boundary conditions regulated by the evaporation rate at the surface and equal to zero at the $R(t)$ depth. (iii) The evolution with time of $R(t)$ is obtained by equating the quantity of deactivated traps, $N_t\,dR$, with the number of interstitials needed to deactivate them, $\phi_{\mathrm{in}}/n_t\,dt$, where ϕ_{in} is the flux towards the active traps that can be calculated on the basis of the *I* concentration profile at time *t*. From the analytical solution of c_I and by Eq. (1), we can calculate $W(x)$, the final broadening of a hypothetical B spike located at a depth *x*, that is, a quantity proportional to the interstitial concentration at *x* integrated over the time *T*. It is expressed by

$$W=\alpha(x-\beta)^2, \tag{3}$$

where

$$\alpha=\frac{n_t N_t}{2}\Big/\frac{D_I c_I^{\mathrm{eq}}}{D_{\mathrm{B}}^{\mathrm{eq}}}, \tag{4a}$$

$$\beta=(r_p+2\lambda)\left[\left(1+\frac{2I_0}{n_t N_t(r_p+2\lambda)}\right)^{1/2}-1\right]+r_p, \tag{4b}$$

and $I_0=\int_0^T\phi(t)dt$ is the number of injected interstitials at the end of TED. This solution is valid in the range $r_p<x<\beta$, where β is the maximum depth at which the interstitials

penetrate after I_0 injection. As can be noted this analytical solution provides a strong simplification of the problem and allows us to point out the exact information that can be obtained by our multi-δ experiment.

First of all, W only depends on the total amount of injected interstitials, I_0, and not on the time evolution of the interstitial release process. In other words, in order to describe the B δ-doping broadening at the end of the TED process, it is not necessary to know the details of the complex phenomena of interstitial release from the implanted zone. Furthermore, the two parameters α and β can be fitted through the experimental data. Once the value of the $(D_I c_I^{eq})/D_B^{eq}$ coefficient is fixed, α gives information about the product $n_t N_t$, which is the interstitial concentration that can be absorbed by a N_t trap density or, in other words, the effective number of sites that can trap interstitials; on the other hand, β can give information about the evaporation length λ after having set the r_p and I_0 values.

In Fig. 8(b) the analytical fit to the data of our test structure is shown (—). A comparison with a numerical calculation of the full set of equations is also reported (···), attesting the good degree of approximation of the analytical solution. As previously pointed out, the numerical solution implies the assumption of many more physical quantities than the analytical solution; the results of both methods strictly agree for any reasonable choice of the physical quantities providing the same values of α and β in Eqs. (4). Both the analytical and numerical fit to the experimental data of Fig. 8(b) give $n_t N_t = (5.5 \pm 2.0) \times 10^{16}\,\mathrm{cm}^{-3}$ and $\lambda = 10 \pm 10$ nm. The error bars are obtained by taking into account the range of the $(D_I c_I^{eq})/D_B^{eq}$ coefficient given in the literature[1,5,40–42] and assigning a 30% error to the ion projected range r_p (~30 nm) as calculated by simulation of the TRIM code, "Transport of Ion in Matter."[43] The injected interstitials, I_0, are assumed to be equal to the implant fluence, as given by the plus-one model.[12] The obtained results indicate that the number of traps in our material is relatively low if compared to other proposed experiments,[4,16] indicating the good quality of the growth. The λ value is very close to zero, indicating that the surface acts as a very efficient interstitial sink.

Summarizing, the model developed is able to simulate the diffusion of injected interstitials into our MBE-grown material, taking into account and evaluating both the intrinsic traps for interstitials and the surface recombination effect.

B. Self-interstitial–carbon interaction

At this point, the obtained $n_t N_t$ and λ values are the key numbers in order to determine the number of interstitials employed to deactivate the traps during the migration into the bulk, and the number of I's lost through the surface, respectively. These inputs will be fundamental in the following to compute the number of I's that effectively interact with the substitutional C in the $Si_{1-y}C_y$ layers. The equations regulating the trap-limited diffusion of interstitials can also be used to model the interaction between C and I. In fact, the model can be applied to our samples with a C-rich layer after some preliminary considerations. The experimental results described in the preceding section point out two

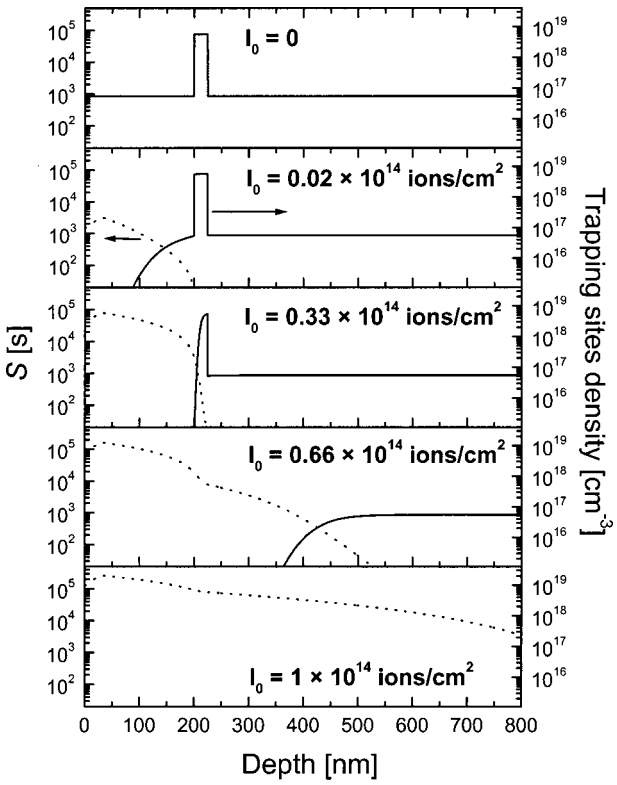

FIG. 9. Results of numerical simulations. As a function of the depth x, the interstitial supersaturation integrated over the I injection time (S) (···, left-hand scale) and the trapping site density ($n_C N_C + n_t N_t$, —, right-hand scale) are plotted for different amounts of injected interstitials, I_0. The first panel shows the starting trapping site density. $n_t N_t$ is obtained by the fit of Fig. 8(b), N_C is given by the SIMS analysis for the $3.4 \times 10^{13}\,\mathrm{C/cm}^2$ sample, while n_C is set equal to 0.4. The following panels show the evolution of the Is migration and the trap filling by increasing the total dose of injected interstitials.

important facts: (i) in our regime, the C in the layer mainly undergoes clustering rather than out-diffusion (Fig. 6), suggesting that C can be considered, in a first approximation, as a nondiffusive trap; (ii) after the clustering process C is not able to capture further interstitials and the clusters result to be very stable. This fact suggests that the backward reaction (interstitial release by cluster) can be neglected.

As C can be considered as a nondiffusive trap, the trap density emerges as the sum of a background of intrinsic traps (just characterized in the preceding paragraph) plus the C concentration in the $Si_{1-y}C_y$ layer (N_C). Furthermore, Eqs. (2) have to be upgraded with the addition of a new equation for the carbon traps similar to that for the intrinsic traps [Eq. (2b)]. The main difference with the previous case is that now the C-trap concentration (N_C) is known by the SIMS and HRXRD measurements, and information about n_C (i.e., the number of interstitials captured by each C atom) can be obtained by fitting the experimental data.

Figure 9 reports the results of a numerical simulation obtained considering a C box profile similar to the sample with $3.4 \times 10^{13}\,\mathrm{C/cm}^2$ (C concentration of $1.5 \times 10^{19}\,\mathrm{C/cm}^3$ in a region 25 nm thick, placed 200 nm below the surface). For

these simulations n_C was assumed to be 0.4, which will be later demonstrated to be a reasonable value for this sample. The model is able to predict the I concentration as a function of depth for various implantation doses. In this graph S ($\cdots$, left-hand scale) is the interstitial supersaturation (i.e., I concentration normalized to the equilibrium one) integrated over the I-injection time. As soon as traps are deactivated by capturing the incoming interstitials, the density of active trapping sites ($n_C N_C + n_t N_t$, intrinsic plus carbon,—, right-hand scale) decreases, as can be seen from the same plot. The active trap front is not abrupt in the numerical calculations because it depends on the interstitial penetration length, $1/\sqrt{4\pi a_t N_t}$, which does not enter into the analytical calculations. In Fig. 9, for the simulations, the capture radius a_t has been assumed to be $a_t = 0.5$ nm. The value of the capture radius only influences the shape of the deactivation front, but it does not affect the calculated supersaturation. The different panels correspond to increasing amounts of injected interstitials, I_0. The first panel with $I_0 = 0$ illustrates the initial concentration of active trapping sites. For a low interstitial dose ($I_0 = 0.02 \times 10^{14}$ ions/cm^2), only intrinsic traps in the first 200 nm are deactivated and the S increases only in the Si cap layer. Increasing I_0, we note that the interstitials begin to interact with C and, due to the high C dose, a large amount of injected interstitials is used to deactivate C; in the meantime, the supersaturation continues to increase in the Si cap layer. Until I_0 is less than 0.33×10^{14} ions/cm^2, no interstitial is able to go beyond the C-rich layer, and the interstitial concentration remains at the equilibrium value for depths greater than 200 nm. When the injected interstitial dose is increased to 0.66×10^{14} ions/cm^2, the C traps are fully deactivated, and the interstitial migration overcomes the $Si_{1-y}C_y$ layer and determines an increase of S at depth higher than 200 nm. Finally, for $I_0 = 1 \times 10^{14}$ ions/cm^2 the I migration occurs at depth greater than 800 nm and no active traps are contained within this thickness. The panels in Fig. 9 represent in a pictorial view the situation in terms of I supersaturation and active I traps at the end of the injection of different interstitial amounts. With increasing amount of injected interstitials (I_0), the interstitial front penetrates further and further into the sample. The depth at which interstitials can arrive depends on the number of traps present. Once previous traps are filled by interstitials, they are deactivated (both intrinsic and C-related traps) and the interstitial front can penetrate deeper into the sample. This explains the physics present in the experiment reported in the Sec. III. In fact, the boron broadening W is related to the interstitial supersaturation by Eq. (1).

The first result of the model is also in very good agreement with our experimental data. In fact, for the 3.4×10^{13} C/cm^2 sample (Fig. 4), after ion implantation and annealing, no broadening of the B spike was observed, except for the 1×10^{14} ions/cm^2 implant dose. For smaller implant doses, the interstitial front migration is expected to be blocked into the $Si_{1-y}C_y$ layer, being just involved in the deactivation of the C traps, while a dose of 1×10^{14} ions/cm^2 is high enough to overcome the C-rich region and to cause interstitial supersaturation at depths greater than 800 nm. Moreover, HRXRD analyses revealed that for this sample, in the case of the lowest implant dose (2×10^{13} atoms/cm^2), there is a limited loss of substitutional carbon (about one-third of the total C), while after the 5×10^{13} ions/cm^2 implantation and annealing, the substitutional carbon is below the detection limit, i.e., the loss of substitutionality is almost complete. This means that for the lowest implantation fluence, interstitials just start to interact with the $Si_{1-y}C_y$ layer, being trapped and displacing C out of substitutional sites, but the I migration is blocked into the $Si_{1-y}C_y$ membrane. In the second case, most of C traps are deactivated and the interstitial front is at the back interface of the $Si_{1-y}C_y$ membrane, but the interstitial flow does not yet arrive to the B spike [see Fig. 3(b)].

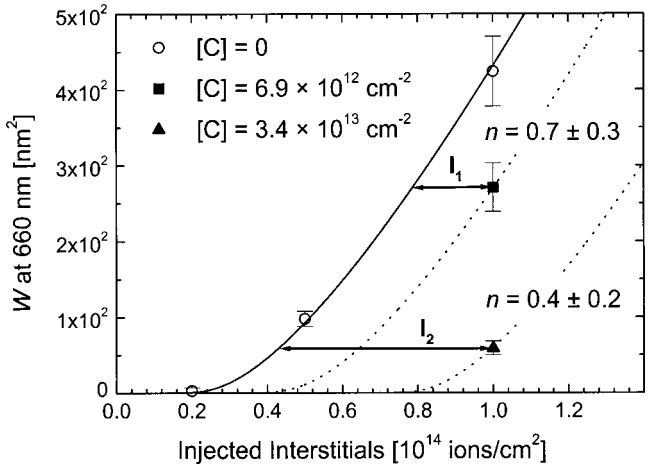

FIG. 10. Broadening of a 660-nm-deep B spike vs injected interstitial dose. The symbols refer to experimental data for the reference sample without C (○) and for the C-rich samples (■ for 6.9×10^{12} C/cm^2, ▲ for 3.4×10^{13} C/cm^2). The continuous line (—) represents the model results for the reference sample. The dotted lines ($\cdots$) are the model fit in the case of C-rich samples. I_1 and I_2 quantify the excess in interstitial injection needed to obtain in the C-rich samples the same broadening as in the reference sample.

On the basis of these results, for a fixed trap density (either intrinsic or intrinsic plus C), it is possible to calculate W, the broadening that a hypothetical B δ-doped layer is predicted to experience at the fixed depth as a function of injected interstitials I_0. In particular, we are interested in the broadening at the depth of 660 nm, where the B spike is positioned in our experiment. In Fig. 10 this quantity is plotted as a function of the injected interstitials. The lines refer to different trap distributions (i.e., different C content), while the symbols refer to experimental values. In particular, for the reference sample without C, the continuous line (—) represents the model result and the open circles (○) are the W values at different implant doses. A perfect agreement between the model and the data is obtained. It is worth noting that, for the implant dose of 2×10^{13} ions/cm^2, no broadening of the boron marker is predicted because the injected interstitials are not enough to deactivate all of the intrinsic traps shallower than the boron marker and hence do not reach the marker itself. This fact is in perfect agreement with the results reported in Fig. 4 for the 2×10^{13} ions/cm^2 implant dose.

The closed symbols in Fig. 10 represent the W values for the lowest- and medium-C-dose samples at 1×10^{14} ions/cm^2 implant dose. These data can be fitted by the model assuming the C-trap profile (N_C) as given by the SIMS profile and using n_C as a fitting parameter. In this way, the model produces a W curve translated towards higher injected interstitial doses ($\cdots$). The amount of the translations (I_1 and I_2) quantifies the excess injection needed to deactivate the C barrier. During this stage of the injection the interstitial front is stopped by the $Si_{1-y}C_y$ layer. Of course, part of the injected interstitials is lost through the surface due to the low value of λ, the surface recombination length. So, the number of I's actually interacting with the $Si_{1-y}C_y$ layer is γI_1 (or γI_2), where $\gamma=0.2\pm0.1$ is the inward fraction of the I flux. Therefore, the number of interstitials needed to fully deactivate the $Si_{1-y}C_y$ layers is $(4.8\pm2.4)\times10^{12}$ and $(12.5\pm6.3)\times10^{12}\,I/\text{cm}^2$ for the low and medium C dose, respectively. These data lead to values of $n_C=0.7\pm0.3$ for the samples with 6.9×10^{12} C/cm^2 and $n_C=0.4\pm0.2$ for the samples with 3.4×10^{13} C/cm^2.

The model developed for the injected interstitial diffusion limited by intrinsic traps is able to simulate I diffusion even in the case of carbon traps. In fact, using a numerical simulation we showed the path of the interstitial migration front from the I source to the bulk of the sample through a $Si_{1-y}C_y$ layer. Moreover, in this manner it was possible to evaluate the number of interstitials that actually interact with C atoms.

C. Atomistic interpretation

According to the above results, it appears that each interstitial is able to deactivate about two substitutional C atoms ($n_C=0.5$). This gives the stoichiometric ratio between I and C_s to produce nonsubstitutional, clustered carbon C_{cl} through the following reaction:

$$I+2C_s\rightarrow 2C_{cl},$$

where according to our experimental results (see Fig. 7), the immobile clustered carbon C_{cl} is no longer active as an interstitial trap.

The reaction above allows a microscopical interpretation described by the following well-known two-step trapping and clustering reactions:[12,20,30,31]

$$I+C_s\rightarrow C_i\,,$$

$$C_s+C_i\rightarrow(C_sC_i)$$

where in the first ''kick-out'' reaction a substitutional carbon (C_s) traps a self-interstitial (I), producing a highly mobile interstitial carbon (C_i). Following the second reaction, the mobile C_i does not undergo an out-diffusion[21,24] but, interacting with a substitutional C_s, stops its motion and forms an immobile couple C_sC_i.[37,44,45] According to the interpretation above, the C traps are deactivated in the immobile couple C_sC_i. In this manner, one self-interstitial is trapped and is able to deactivate two C traps, by means of the trapping and clustering reactions. The absence of C out-diffusion and the evidence of C precipitation could be explained in terms of the high I flux, which moves both the reactions above toward the right-hand side.

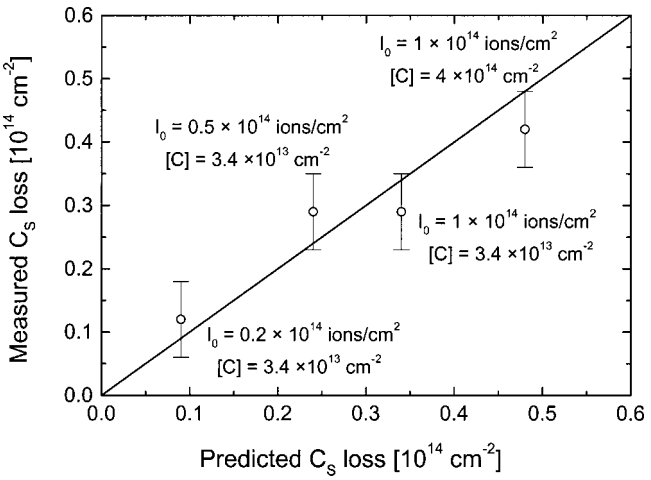

FIG. 11. HRXRD measured loss of substitutional carbon vs the simulated one, assuming our model with $n_C=0.5$. The continuous line (—) is a straight line with slope 1. A linear fit (not shown) of the data points by means of a straight line through the origin of the axes yields a slope of 0.9 ± 0.1.

A further, independent evaluation of n_C is obtained by comparing the amount of deactivated C atoms as predicted by the model to the number of C atoms removed from substitutional sites (giving no contribution to the strain), as experimentally measured by HRXRD. In Fig. 11 the results of four samples are reported, in terms of substitutional C loss, measured by HRXRD, versus deactivated C traps, predicted by the model with $n_C=0.5$. HRXRD analyses revealed a reduction of strain and therefore a reduction of the substitutional C concentration with respect to the as-grown samples. This is due to the fact that the interstitial front has interacted with C and has deactivated at least a part of the initial substitutional C. As can be noted in Fig. 11 the measured loss of substitutional C and the predicted deactivated C traps can be considered equal inside the error bars (the continuous line is indeed a straight line with slope 1). Since the model calculation is performed in the hypothesis of $n_C=0.5$, this result gives a further and independent confirmation of this ''stoichiometric'' ratio during the reactions between Si self-interstitials and substitutional C in the case of interstitials injected by ion implantation.

V. CONCLUSIONS

The mechanism of self-interstitials trapping by substitutional carbon in silicon was studied. In particular, the ability of a $Si_{1-y}C_y$ layer, interposed between the near-surface self-interstitial source and a deep B spike, to filter the interstitial flow towards the bulk and, consequently, to strongly reduce the boron-enhanced diffusion, has been shown. This trapping ability is related to the total C dose in the $Si_{1-y}C_y$ membrane. Moreover, once having trapped the self-interstitials, the substitutional carbon atoms lose their substitutional sites but cannot diffuse away. In fact, no C out-diffusion was ob-

served, and C atoms that have interacted with self-interstitials precipitate into the C-rich region, showing a high thermal stability. Furthermore, these immobile C atoms are unable both to interact with other interstitials and to release the trapped interstitials. So, C emerges as an efficient sink for Si interstitials only if they are on substitutional sites; moreover, after the trapping reaction this condition is lost, and the C atoms are no longer able to interact with new self-interstitials. In order to characterize the interactions between the C traps and the Si interstitials, a model describing the implanted interstitial migration was developed, taking into account the surface recombination, the presence of intrinsic traps within the material, and the presence of C traps. The model is able to predict the broadening of a B spike that experiences an interstitial supersaturation due to ion implantation. The interstitial front coming from the implanted region is seen to penetrate deeper and deeper through trap deactivation, and eventually for high interstitial values it reaches the deep B spike. By a comparison with the experimental data, the amount of *I*'s that actually interact with C atoms was estimated, and an atomistic interpretation of the C-*I* reaction was given. In fact, by fitting experimental data with the model, it was found that one Si interstitial is able to deactivate two C traps. The interaction between Si interstitials and C is supposed to proceed sequentially by means of *I* trapping and C clustering reactions.

ACKNOWLEDGMENTS

The authors wish to thank L. Colombo and F. Bernardini (INFM–Cagliari University) for very useful discussions, A. Marino (CNR-IMETEM) and R. Storti (University of Padova) for expert technical assistance, and S. Pannitteri, C. Bongiorno, and C. Spinella (CNR-IMETEM) for TEM analyses. This work has been partially supported by MURST through the project COFIN 2000.

[1] P. M. Fahey, P. B. Griffin, and J. D. Plummer, Rev. Mod. Phys. **61**, 289 (1989).
[2] N. E. B. Cowern, K. T. F. Janssen, G. F. A. van de Walle, and D. J. Gravesteijn, Phys. Rev. Lett. **65**, 2434 (1990).
[3] N. E. B. Cowern, G. F. A. van de Walle, D. J. Gravesteijn, and C. J. Vriezema, Phys. Rev. Lett. **67**, 212 (1991).
[4] N. E. B. Cowern, Appl. Phys. Lett. **64**, 2646 (1994).
[5] H. Bracht, N. A. Stolwijk, and H. Mehrer, Phys. Rev. B **52**, 16 542 (1995).
[6] H. Bracht, E. E. Haller, and R. Clark-Phelps, Phys. Rev. Lett. **81**, 393 (1998).
[7] T. Y. Tan and U. Gösele, Appl. Phys. A: Solids Surf. **37**, 1 (1985).
[8] H.-J. Gossmann, T. E. Haynes, P. A. Stolk, D. C. Jacobson, G. H. Gilmer, J. M. Poate, H. S. Luftam, T. K. Mogi, and M. O. Thompson, Appl. Phys. Lett. **71**, 3862 (1997).
[9] J. Zhu, T. Diaz de la Rubia, L. H. Yang, C. Mailhiot, and G. H. Gilmer, Phys. Rev. B **54**, 4741 (1996).
[10] B. Sadigh, T. J. Lenosky, S. K. Theiss, M.-J. Caturla, T. Diaz de la Rubia, and M. A. Foad, Phys. Rev. Lett. **83**, 4341 (1999).
[11] W. Windl, M. M. Bunea, R. Stumpf, S. T. Dunham, and M. P. Masquelier, Phys. Rev. Lett. **83**, 4345 (1999).
[12] P. A. Stolk, J. H.-J. Gossmann, D. J. Eaglesham, D. C. Jacobson, C. S. Rafferty, G. H. Gilmer, M. Jaraiz, J. M. Poate, H. S. Luftman, and T. E. Haynes, J. Appl. Phys. **81**, 6031 (1997), and references therein.
[13] H. S. Chao, P. B. Griffin, J. D. Plummer, and C. S. Rafferty, Appl. Phys. Lett. **69**, 2113 (1996).
[14] E. Napolitani, A. Carnera, E. Schroer, V. Privitera, F. Priolo, S. Moffatt, Appl. Phys. Lett. **75**, 1869 (1999).
[15] H. Saleh, M. E. Law, S. Bharatan, K. S. Jones, V. Krishnamoorthy, and T. Buyuklimanli, Appl. Phys. Lett. **77**, 112 (2000).
[16] P. A. Stolk, D. J. Eaglesham, H.-J. Gossmann, and J. M. Poate, Appl. Phys. Lett. **66**, 1370 (1995).
[17] J. P. Kalejs, L. A. Ladd, and U. Gösele, Appl. Phys. Lett. **45**, 268 (1984).
[18] P. Werner, H. Gossmann, D. C. Jacobson, and U. Gösele, Appl. Phys. Lett. **73**, 2465 (1998).
[19] R. F. Scholz, P. Werner, U. Gösele, and T. Y. Tan, Appl. Phys. Lett. **74**, 392 (1999).
[20] G. D. Watkins and K. L. Brower, Phys. Rev. Lett. **36**, 1329 (1976).
[21] R. Scholz, U. Gösele, J.-Y. Huh, and T. Y. Tan, Appl. Phys. Lett. **72**, 200 (1998).
[22] H. Rücker, B. Heinemann, W. Röpke, R. Kurps, D. Krüger, G. Lippert, and H. J. Osten, Appl. Phys. Lett. **73**, 1682 (1998).
[23] N. E. B. Cowern, A. Cacciato, J. S. Custer, F. W. Saris, and W. Vandervorst, Appl. Phys. Lett. **68**, 1150 (1996).
[24] H. Rücker, B. Heinemann, D. Bolze, R. Kurps, D. Krüger, G. Lippert, and H. J. Osten, Appl. Phys. Lett. **74**, 3377 (1999).
[25] M. S. Carroll, C-L. Chang, J. C. Sturm, and T. Büyüklimanli, Appl. Phys. Lett. **73**, 3695 (1998).
[26] E. Napolitani, A. Coati, P. De Salvador, A. Carnera, S. Mirabella, S. Scalese, and F. Priolo, Appl. Phys. Lett. **79**, 4145 (2001).
[27] J. W. Strane, H. J. Stein, S. R. Lee, S. T. Picraux, J. K. Watanabe, and J. W. Mayer, J. Appl. Phys. **76**, 3656 (1994).
[28] G. G. Fischer, P. Zaumseil, E. Bugiel, and H. J. Osten, J. Appl. Phys. **77**, 1934 (1995).
[29] D. De Salvador, E. Napolitani, A. Coati, M. Berti, A. V. Drigo, M. S. Carroll, J. C. Sturm, J. Stangl, G. Bauer, and L. Lazzarini, in *Si Front-End Processing-Physics and Technology of Dopant-Defect Interactions III*, edited by K. Jones *et al.*, Mater. Res. Soc. Symp. Proc. No. 669 (Materials Research Society, Warrendale, 2001).
[30] L. W. Song, X. D. Zhan, B. W. Benson, and G. D. Watkins, Phys. Rev. B **42**, 5765 (1990).
[31] J. L. Ngau, P. B. Griffin, and J. D. Plummer, J. Appl. Phys. **90**, 1768 (2001).
[32] F. Priolo, G. Mannino, M. Miccichè, V. Privitera, E. Napolitani, and A. Carnera, Appl. Phys. Lett. **72**, 3011 (1998).
[33] M. Berti, D. De Salvador, A. V. Drigo, F. Romanato, J. Stangl, S. Zerlauth, F. Schäffler, and G. Bauer, Appl. Phys. Lett. **72**, 1602 (1998).
[34] D. De Salvador, M. Petrovich, M. Berti, F. Romanato, E. Napolitani, A. V. Drigo, J. Stangl, S. Zerlauth, M. Muhlberger, F. Schaffler, and G. Bauer, Phys. Rev. B **61**, 13 005 (2000).

[35] P. F. Fewster and C. Curling, J. Appl. Phys. **62**, 4154 (1987).
[36] R. B. Fair, in *Impurity Doping Processes in Si*, edited by F. F. Y. Wang (North-Holland, Amsterdam, 1981), p. 315.
[37] J. Tersoff, Phys. Rev. Lett. **64**, 1757 (1990).
[38] This term could be assumed to be very small (zero) in the case of our samples. This was tested by annealing the test structure for different times after exhausting the TED. In no case was anomalous B-peak broadening detected due to the release of interstitials by the traps saturated during TED.
[39] D. R. Lim, C. S. Rafferty, and F. P. Clemens, Appl. Phys. Lett. **67**, 2302 (1995).
[40] Y. Haddara, B. T. Folmer, M. E. Law, and T. Buyuklimanli, Appl. Phys. Lett. **77**, 1976 (2000).
[41] N. A. Stolwijk, J. Holzl, W. Frank, E. R. Weber, and H. Mehrer, Appl. Phys. A: Solids Surf. **39**, 37 (1986).
[42] S. Mantovani, F. Nava, S. Nobili, and G. Ottaviani, Phys. Rev. B **33**, 5536 (1986).
[43] J. P. Biersack and L. G. Haggmark, Nucl. Instrum. Methods **174**, 257 (1980).
[44] G. Davis and R. C. Newman, in *Handbook of Semiconductors*, 2nd ed., edited by S. Mahajan (North-Holland, Amsterdam, 1994), Vol. 3, p. 1557.
[45] U. Gösele, P. Laveant, R. Scholz, N. Engler, and P. Werner, in *Si Front-End Processing-Physics and Technology of Dopant-Defect Interactions II*, edited by A. Agarwal *et al.*, Mater. Res. Soc. Symp. Proc. No. 610 (Materials Research Society, Warrendale, 2000).